

Travel time and source variation explain the molecular transformation of dissolved organic matter in an Alpine stream network

H. Peter^{1*}, G. Singer², A. J. Ulseth^{1,3}, T. Dittmar^{4,5}, Y. T. Prairie⁶, and T.J. Battin¹

¹ Stream Biofilm and Ecosystem Research Laboratory, School of Architecture, Civil and Environmental Engineering, Ecole Polytechnique Fédérale de Lausanne, CH-1015 Lausanne, Switzerland

² Leibniz-Institute of Freshwater Ecology and Inland Fisheries, 12587 Berlin, Germany

³ Department of Biological Sciences, Sam Houston State University, Huntsville, Texas, 77341 USA

⁴ Institute for Chemistry and Biology of Marine Environment (ICBM), ICBM-MPI Bridging, Group for Marine Geochemistry, 26129 Oldenburg, Germany

⁵ Helmholtz Institute for Functional Marine Biodiversity at the University of Oldenburg (HIFMB), 26129 Oldenburg, Germany

⁶ Groupe de Recherche Interuniversitaire en Limnologie, (GRIL), Département des Sciences Biologiques, Université du Québec à Montréal, Montréal, Québec, Canada

Corresponding author: Hannes Peter (hannes.peter@epfl.ch)

Key Points:

- Discharge-weighted travel time explains the spatial variation of DOM composition at the molecular level in a stream network.
- Seasonal differences in DOM composition relate to different source materials.
- The distribution of sources, mixing at confluences and the oxidative state of DOM are important drivers of the spatial DOM dynamics.

Abstract

Streams and rivers are important components of the carbon cycle as they simultaneously transport and transform terrigenous dissolved organic matter (DOM). The time DOM spends in a stream network is an important constraint on the biogeochemical processes that act upon DOM. We used high-resolution Fourier-Transform Ion Cyclotron Resonance Mass Spectrometry (FT-ICR MS) to study the spatial distribution of DOM at the molecular level at more than 100 sites within an Alpine stream network during summer and winter baseflow. We developed a model approximating the time DOM spent in the fluvial network. Discharge-weighted travel time (DWTT) explained the compositional changes of DOM, which differed markedly in summer and winter. We attribute the seasonal differences to differences in source material. Hydrological mixing at confluences was an important driver of the spatial dynamics of DOM. From the spatial patterns of individual DOM compounds we inferred the distribution of sources within the catchment, which differed seasonally. Finally, we estimated the apparent mass transfer coefficients of individual DOM compounds at the network level and identified the oxidative state of DOM as an important factor explaining uptake efficiency. This work contributes to our understanding of the spatial processes, temporal constraints and chemical properties of DOM that regulate the transformation and diagenesis of DOM at the fluvial network scale.

Plain Language Summary

Dissolved organic matter (DOM) represents the largest flux of organic carbon in streams. DOM is composed of thousands of molecules, which are transported, mixed and processed as the water moves through a stream network. Stream network structure and the time DOM is exposed to transformation processes are likely important factors explaining changes in DOM composition. Using a model incorporating travel time and stream network structure, we show how DOM changes in a stream network in the Austrian Alps. Different sources, such as leave litter, and their spatial distribution explain differences between summer and winter. DOM uptake efficiency is related to the oxidative state of molecules. Taken together, this study shows how network

structure and the distribution of apparently reactive DOM compounds drive the spatial dynamics of streamwater DOM.

1 Introduction

Dissolved organic matter (DOM) represents the largest flux of organic carbon in streams (Battin et al., 2008), connecting terrestrial ecosystems and coastal oceans (Regnier et al., 2013). In streams and rivers, DOM sustains the energy flow mediated by heterotrophic bacteria (Hall & Meyer, 1998; Kaplan & Bott, 1983) and – being associated to both primary production and respiration – DOM biogeochemistry is intricately tied to stream ecosystem metabolism (Berggren & del Giorgio, 2015; Bernhardt et al., 2017). This relevance has triggered, already during the early days of stream science, the quest for spatial patterns of DOM chemistry along the fluvial continuum (e.g. Ford et al., 1990; Vannote et al., 1980), which is still pursued today (Creed et al., 2015; Gonsior et al., 2016; Mosher et al., 2015). From these studies we know that the typically terrestrial signatures of DOM in headwaters shift to imprints of in-stream biogeochemical processing in higher-order streams. At the landscape scale, hydrologic averaging as water of diverse sources mixes, changes in terrestrial-aquatic connectivity and biogeochemical processing result in the homogenization of dissolved organic carbon (DOC) concentration (Creed et al., 2015). However, since the advent of ultra-high resolution mass spectrometry analyses it is clear that DOM is a complex mixture of a multitude of compounds (e.g. Kellerman et al., 2014; Kim et al., 2006; Seitzinger et al., 2005). Yet, it remains unclear how the spatial dynamics of individual DOM compounds contribute to DOM dynamics at the fluvial network scale.

The chemical complexity of streamwater DOM results from its diverse sources and the various biological and chemical processes that alter its initial structure (Gonsior et al., 2009; Jaffé et al., 2012; Riedel et al., 2016; Seidel et al., 2015; Sleighter et al., 2014). Comparative analyses using

73 state-of-the art chemical resolution have shown that a large fraction of DOM chemodiversity is
74 shared among streams and rivers (Gonsior et al., 2016; Jaffé et al., 2012; Mosher et al., 2015;
75 Riedel et al., 2016), pointing to the importance of similar sources, such as leaf litter or soil
76 organic matter. The chemical composition of DOM affects its transformation by microorganisms
77 (Lu et al., 2015; Riedel et al., 2016; Sleighter et al., 2014); of particular interest is the
78 observation that oxygen-rich molecules are preferentially degraded by microorganisms (Kim et
79 al., 2006; Singer et al., 2010). At the same time, microbial activity in streams may shift DOM
80 towards molecules with smaller masses (Kim et al., 2006), but potentially also to larger humic-
81 like compounds (Guillemette & del Giorgio, 2012).

82 Besides microbial degradation, sorption to minerals, photochemical degradation and
83 complexation with metals changes DOM composition (e.g. Aiken et al., 2011; Creed et al., 2015;
84 Hunter et al., 2016; Seitzinger et al., 2005). Each of these transformation processes acts on a
85 specific time scale, and in order to better predict the spatial turnover of DOM, these timescales
86 need to be opposed to the velocity of downstream transport. Indeed, residence time can constrain
87 the processing of DOM and has been identified as a prime control on bulk DOM decomposition
88 rate across various freshwater ecosystems and climates (Barnes et al., 2018; Bertuzzo et al.,
89 2017; Casas-Ruiz et al., 2017; Catalán et al., 2016; Hrachowitz et al., 2016).

90 The spatial structure of dendritic stream networks (Benda et al., 2004) has potentially important
91 consequences for DOM chemical composition and dynamics (Kayler et al., 2019). For instance,
92 headwaters, the most abundant streams within fluvial networks, are tightly coupled with the
93 catchment and receive large amounts of terrestrial DOM. As predicted by the River Continuum
94 Concept (Vannote et al., 1980), proximity to terrestrial sources may translate into elevated DOM
95 diversity in upstream reaches, a notion that was recently endorsed by Mosher et al. (2015) and

Creed et al. (2015). Yet, given the high molecular diversity of natural DOM, a better understanding of the spatial patterns and dynamics of DOM composition at the stream network scale, both as a cause and consequence of DOM availability, is required.

We used FT-ICR MS to study the molecular composition of streamwater DOM across more than 110 sites within a subalpine stream network (Ybbs River, Austria), during summer and winter baseflow conditions. We estimated discharge-weighted travel time at any given point in the stream network; discharge-weighted travel time approximates the time DOM spends in the open channel and reflects stream network topology. We hypothesized that streamwater DOC concentration and DOM molecular composition gradually change from the smallest headwaters to the larger streams within the network. This is based on the assumption that some molecules will be preferentially removed *en route* while others may accumulate, which likely is related to intrinsic chemical properties. We further posit that these changes will differ between seasons, as we expect streamwater DOM to reflect the varying contributions from fresh plant material and stream microorganisms (including algae) in summer and degrading leaf litter in winter. Building on the conceptual model of Creed et al. (2015), we expect that the spatial distribution of sources in the network, DOM production and decay and hydrological mixing along flow paths underlie the compositional changes of DOM. Based on the work of Abbott et al. (2017), we therefore explored the reduction of spatial variance of individual DOM compounds, as this is related to the patch size and distribution of sources in the stream network.

Our objectives were to reveal at high spatial and molecular resolution the dynamics of DOM as it moves through the Ybbs river network. To achieve this, we investigated DOM compositional changes along the gradient of discharge-weighted travel time, a measure of residence time accounting for spatial network configuration. We further explored, on a compound level,

seasonal differences in the distribution of sources. Finally, we examined the apparent mass transfer coefficients of individual compounds, which is a measure of uptake independent of changes in stream dimension. We identified the oxidative state of DOM molecules as an important factor explaining apparent DOM mass transfer velocities. Taken together, our analyses show how DOM molecular composition changes from headwater streams to a fifth-order stream as DOM from various sources is transported, mixed and processed. Our study thus contributes to our understanding of how network topology and the distribution of apparently reactive DOM compounds drive the spatial dynamics of DOM.

2 Materials and Methods

2.1 Study sites and sampling

We studied the pre-alpine Ybbs River catchment (254 km²; 47°49'N, 15°04'E) in winter (January 2010; n=115) and summer (September 2011; n=148) (Figure 1). Altitude ranges from 532 to 1893 m above sea level and catchment geology is dominated by dolomite rock. Soils consist of Leptosols at high elevations, Cambisols at mid elevation hillslopes and Gleysols and Fluviosols in valleys that are underlain by alluvial deposits. Vegetation cover consists of 82% forests and 11% alpine meadows; approximately 7% of the total surface area is constituted of settlements with agriculture, as well as bare rock at high elevation. The catchment vegetation is composed of mixed forests (*Picea abies*, *Fraxinus excelsior*, *Fagus sylvatica*, *Acer pseudoplatanus*) and alpine meadows.

In total, we collected streamwater from 38 1st-order, 51 2nd-order, 42 3rd-order, 19 4th-order and from one 5th-order stream. Sampling sites were clustered around confluences to maximize

lengths of reaches between confluences (Figure 1). Samples were collected after extended periods of baseflow to ensure hydrological stability. At each site, we collected up to 4 liters of filtered (GF/F, Whatman, Maidstone, UK, pre-combusted at 450°C for 4 h) streamwater into polypropylene copolymer containers previously soaked with 0.1N HCl and rinsed with Milli-Q water; samples were cooled and transported to the laboratory within 2 hours for extraction. We further measured streamwater electrical conductivity, temperature, dissolved oxygen and pH using a YSI 600R probe (Ohio, U.S.A.) and sampled filtered streamwater (pre-combusted GF/F, Whatman) for the measurement of DOC concentration using a TOC analyzer (GE-Sievers 900) operated with an inorganic carbon removal unit.

2.2 Discharge-weighted travel time

We calculated discharge-weighted travel time (DWTT) by cumulating the time streamwater spends in the open channel along its routing from the smallest headwaters to the outlet of the catchment. First, using a high-resolution (10 x 10 m) digital elevation model (DEM), we predicted discharge at any given point in the Ybbs River network using a previously published scaling relationship between discharge and catchment area (Ceola et al., 2014). The average discharge measured at a reference gauge close to the outlet of the Ybbs River network during the two sampling campaigns (~1 week) served to adjust the modeled discharge to the conditions in summer and winter. Next, we used hydraulic geometry relationships (Leopold & Maddock, 1953) previously established from measurements of channel width, streamwater depth and flow velocity at more than 100 sites across the Ybbs River network (Ceola et al., 2014) to infer flow velocity from discharge. We then calculated the residence time of water in each pixel and linearly cumulated these to travel times along flow paths. At confluences, travel times were

165 weighted according to the contributing discharge from either stream forming the confluence.
166 Thereby, DWTT incorporates the time DOM spends in the open channel and network structure
167 in terms of drainage and confluence density. We recognize that this approach neglects all
168 subsurface lateral water input and does not capture transient storage of water in interstitial,
169 subsurface environments; these two processes would have opposing influences on DWTT. The
170 more than 100 sampling sites were regularly distributed across the entire DWTT gradient
171 (supporting information Figure S1).

173 2.3 Streamwater DOM analysis using FT-ICR MS

174 DOM was extracted from streamwater acidified with HCl p.a. to pH 2 using Bond Elut PPL
175 (Agilent) solid phase extraction cartridges by gravity flow (Dittmar et al., 2008). Water volumes
176 and resin mass were downscaled by a factor 10 for the summer campaign. Following extraction,
177 SPE cartridges were rinsed with MQ water adjusted to pH 2, dried with N₂ and eluted with
178 MeOH (HPLC grade, Sigma). DOM extracts were stored at -20 °C pending analysis by FT-ICR
179 MS. An aliquot was used to measure extraction efficiency. We recognize that very small polar
180 molecules and colloidal aggregates may be lost during extraction; on average, extraction
181 efficiencies were 59±4% and 51±5% (mean±SD) for winter and summer, respectively. SPE
182 extracts were diluted to ~10 ppm in MeOH:MQ at 2:1 (v/v) prior to FT-ICR MS on a 15 Tesla
183 Solarix mass spectrometer (Bruker Daltonics, Billerica, MA, USA) equipped with an
184 electrospray ionization source (Bruker Apollo II). Samples were injected at a rate of 120 µL h⁻¹,
185 ion accumulation was set to 0.45-0.55 s, in-source CID was set to 50 V to fragment dimers in the
186 complex samples. Five hundred scans per sample were accumulated to mass spectra ranging
187 from 150 to 2000 Da, but no peaks were detected for masses >1000 Da. After internal

calibration, raw masslists were exported from Bruker's Data Analysis software at S/N=5 for further data processing using in-house code in R. First, molecular formulae were assigned to m/z values assuming single-charged deprotonated molecular ions and Cl-adducts for a maximum elemental combination of C₁₀₀H₂₅₀O₈₀N₄P₂S₂. This happened for each spectrum individually with (i) a conservative mass tolerance of 0.4 ppm, (ii) commonly assumed restrictions of elemental composition (Lesaulnier et al. 2017), and (iii) a check for isotope confirmation (based on adequate mass shift with a tolerance of 0.4 ppm and adequate intensity ratio(s) of isotopic daughter peaks to the monoisotopic parent peak within 20%). In case of multiple formula assignments to the same peak, we gave preference to formulae with better isotope confirmation (more daughter peaks), and formulae involved in longer homologous series based on CH₂ (aliphatic elongation), CO₂ (acid-based elongation) or both (2D-molecular network) in this ranked order. Confirmed formulae were then assembled to a database of chemically feasible compounds. In a second stage of data processing, peaks from all spectra were then reassigned to formulae in the database, neglecting isotope confirmation to recover low-intensity peaks, and resulting in a peak alignment across spectra based on assigned formulae rather than observed m/z. A sizeable number of formulae could then be ruled out by applying a refined mass tolerance computed as a standard error of the mean $0.6/\sqrt{n}$, where 0.6 ppm is an estimated maximum error for low S/N peaks and n is the frequency of occurrence across all spectra. Eventually existing multiple assignments were resolved by quality of isotope confirmation (i.e., across a greater number of spectra) and average length of homologous series. Last, intensities of formulae found in deprotonated charged state and as a Cl-adduct were summed, and dominant (S/N>20) peaks identified in blank samples (MQ-water process blank) were deleted.

Molecular formulae were assigned to categories based on their elemental composition (black carbon, unsaturated and highly unsaturated aliphatics, saturated fatty acids, polyphenols, sugars and peptides) and aromaticity was estimated with the modified aromaticity index (Koch & Dittmar, 2006). Further, we classified molecular formulae based on their occurrence in samples obtained in summer and winter, respectively. We considered molecular formulae found in less than 50 % of the samples in both seasons as rare. On the other hand, formulae found in more than half of the sites in summer and winter were classified as common. Molecular formulae common in summer but not in winter and *vice versa* were classified as season-specific. Finally, we calculated the nominal oxidative state of carbon for each formula following Riedel et al. (2012):

$$NOSC = 4 - \left[\frac{4C + H - 3N - 2O - 2S}{C} \right],$$

where C, H, N, O and S are the stoichiometric numbers of carbon, hydrogen, nitrogen, oxygen and sulfur atoms. NOSC therefore describes the average oxidation state of a molecule without regarding its chemical structure.

3 Statistical analyses

We used Generalized Additive Models for Location, Scale and Shape (GAMLSS) implemented in the R package *gamlss* (Rigby & Stasinopoulos, 2005) to model streamwater DOC concentration, electrical conductivity and the relative contribution of DOM populations throughout the network. GAMLSS allows regression-like modeling of response variables which exhibit variance heterogeneity (i.e., the shape of the distribution of the response variable changes with the explanatory variable). To increase comparability (e.g., between DOC concentration and electrical conductivity), we z-transformed the response variables such that the mean of

transformed data equals zero and the standard deviation of transformed data equals one. We then modeled z-scores as a function of DWTT assuming normally distributed errors and using an identity link for the means and cubic splines for standard deviations as additive terms. *gamlss* maximized the penalized likelihood using the RS algorithm. We visualized the model means as well as 10 and 90% percentiles.

We quantified spatial structure of DOC concentration and electrical conductivity using Torgegrams, a special form of empirical semivariograms accounting for flow-connected and flow-unconnected distances as implemented in the SSN package (Ver Hoef et al., 2014) in R. For this, we first used the openSTARS toolbox to derive the Ybbs stream network from a 10 x 10 m digital elevation model and to calculate the spatial information required to fit spatial statistical models. Torgegrams describe spatial structure by means of spatial autocorrelation as a function of stream network distance. We standardized semivariance to increase comparability among DOC and electrical conductivity. Torgegrams show a number of features (McGuire et al., 2014), including the characteristic range of spatial patchiness as the distance corresponding to the inflection point of semivariance.

We investigated the compositional changes in DOM along the DWTT gradient using a combination of canonical correlation analysis, PLS modeling and direct correlation of relative molecular intensities with DWTT. Compositional changes along the travel time gradient were explored by using Canonical Analysis of Principal Coordinates (CAP) (Singer et al., 2012) as implemented in the R package *vegan* (Oksanen et al., 2013). This consists of three steps: Computation of a Bray-Curtis dissimilarity matrix to achieve a representation of relative intensity data of adequate dimensionality, translating it into Euclidean space by means of a Principal Coordinates Analysis (PCoA), and applying Canonical Correlation Analysis (CCorA)

to formally test for an association between DWTT and DOM composition. We further explored potential links between the molecular composition of DOM composition and DWTT using a Partial Least Squares (PLS) model as implemented in JMP Pro 14. We expressed DWTT on a logarithmic scale to distribute the study streams more uniformly across this gradient. PLS is well-suited for datasets with large numbers of potentially colinear predictive variables. However, PLS models are prone to overfitting and we proceeded in two steps to minimize this potential caveat. First, we used k-fold cross-validation to determine the most parsimonious number of PLS components and to identify the molecular formulae that were most important in the model using the VIP score (Eriksson et al., 2006). Second, we randomly excluded 30% of the data as a validation set and fitted a 6-component PLS model using only the molecular formulae with high VIP (>1.5 , 329 out of 4283 formulae) to the remaining training dataset.

We estimated the rate of decrease of variance along the DWTT gradient to identify molecular populations that converge to the catchment-scale average. We calculated the absolute residual intensity of every formula from its catchment-level average. Since hydrological averaging leads to convergence to the catchment average, this procedure typically converted the funnel-like distribution of raw intensity values into a triangular distribution with high residuals at the low end of the DWTT gradient and *vice versa* with low residuals at high DWTT values. We then estimated the rate of convergence by identifying pareto-optimal points on the triangular distribution. These are points for which no other higher value of absolute residual intensity exists at higher DWTT. When more than four pareto-optimal points were found, we fitted a linear model to these points and interpreted the slope as the rate of convergence. A steeper reduction of the triangular distribution outlined by the pareto-optimal front thus indicates a faster convergence to the catchment-scale average.

Finally, given the relative nature of FT-ICR MS data and the averaging of multiple structural isomers behind each formula we estimated *apparent* mass transfer coefficients $v_{f\ app}$ for individual molecular formulae. $v_{f\ app}$ was calculated from changes along reaches between confluences that were sampled in both seasons. Reaches were located between confluences, with the upstream site of a reach being below a confluence and the downstream site of a reach being above the consecutive confluence. To exclude major changes associated to lateral inputs, we inspected differences in electrical conductivity between up- and downstream sites and excluded 2 reaches with >20% difference in conductivity in summer and 4 reaches in winter, resulting in a total number of 31 and 29 estimates of $v_{f\ app}$ for more than 1100 molecular formulae in summer and winter, respectively. $v_{f\ app}$ was calculated as:

$$v_{f\ app} = \frac{\ln(I_1) - \ln(I_2)}{\Delta DWTT} * h,$$

where I_1 and I_2 are the relative peak intensities of a given molecule at the up- and downstream sites of each reach, respectively, $\Delta DWTT$ is the difference in DWTT and h is average water depth. We then averaged all estimates of $v_{f\ app}$ to achieve a measure of network-wide average vertical uptake velocity of individual compounds and multiplied $v_{f\ app}$ with -1, such that negative values indicating compound removal and positive values indicating compound generation. $v_{f\ app}$ assumes units of mm min^{-1} . Estimating compound mass transfer from FT-ICR MS signal intensities assumes that signal intensity is essentially linearly related to the concentration of isomeric mixtures of compounds, an assumption that is typically met as long as the sample matrix is similar (Mostovaya et al., 2017; Seidel et al., 2015). However, differences in ionization efficiency in negative ESI mode, the relative nature of FT-ICR MS data and internal averaging of isomeric compounds are the main limitations of this approach. Moreover, we opted against translating relative peak intensities to absolute data due to measurement noise in both the DOC

concentration and extraction efficiency data. Therefore, and considering that lateral inputs as well as the simultaneous production and degradation may contribute to changes in signal intensity across reaches, $v_{f\ app}$ should be considered as an *apparent* mass transfer rather than a quantitative measure of compound kinetics.

4 Results

4.1 DWTT Distribution

We estimated DWTT as it combines important aspects relevant for DOM dynamics regarding the time DOM spends in a stream network and the spatial configuration of the network. At the stream network scale, median DWTT was 220 min in summer and 259 min in winter. Due to higher discharge and flow velocities in summer, water and DOM moved more rapidly through the Ybbs River network than in winter (paired T-Test, $t=5.59$, $p<0.01$). This translated into a lower DWTT at the catchment outlet in summer (1602 min) than in winter (1890 min) (supporting information Figure S1). In summer, DOM spent on average 104 ± 88 min in 1st order streams. For the same season, the time spent in the network increased on average to 294 ± 183 minutes in 2nd order streams, to 473 ± 185 min in 3rd order and to 1183 ± 344 min in 4th order streams. The importance of spatial network configuration is highlighted by the fact that maximum DWTT in the Ybbs River network (1743 and 2057 min in summer and winter, respectively) is reached in the 4th order mainstem, just before it mixes with relatively “younger” stream water from a subcatchment to form the 5th order stream at the catchment outlet.

4.2 Spatial patterns of streamwater DOC concentration

We contrasted the distribution of streamwater electrical conductivity as a conservative tracer with that of DOC concentration across the DWTT gradient. Average DOC concentration was higher in summer ($1.787 \pm 0.691 \text{ mg C L}^{-1}$) than in winter ($1.238 \pm 0.445 \text{ mg C L}^{-1}$). Variance of both electrical conductivity and DOC concentration decreased with increasing DWTT (Figure 2 A, B, GAMLSS, $p < 0.01$) pointing to hydrological mixing as an important control. For instance, during summer the 25% quantile of sites with lowest DWTT differed on average by $0.784 \text{ mg C L}^{-1}$ from the network average DOC concentration. The 25% quantile of sites close to the outlet had significantly lower differences from the network average (average difference: $0.387 \text{ mg C L}^{-1}$; Welch T Test, $t = 3.61$, $p < 0.01$). Electrical conductivity and DOC concentration converged symmetrically to the overall mean, suggesting equi-proportional mixing of the diverse headwater sources. In contrast to electrical conductivity, the central tendency of DOC concentration along the DWTT gradient was negative during both seasons (GAMLSS, $p < 0.01$), suggesting DOC is removed from the streamwater as it moves through the Ybbs River network. In summer, modeled average DOC concentration decreased by 47.2% from the uppermost to the lowest site in the catchment. In winter, average DOC concentration decreased by 30.2% between those sites. Using geostatistical tools we found that in both seasons electrical conductivity and DOC exhibited signs of spatial patchiness with a characteristic range of 10 to 20 km between both flow-connected and flow-unconnected sites (Figure 2 C, D). Below this distance, semivariance tended to be low, a sign of spatial correlation and hence patchiness. Comparing semivariance for flow-connected and flow-unconnected separation distances, electrical conductivity appeared to be more strongly controlled by transport processes (i.e. higher semivariance among flow-unconnected sites than among flow-connected sites) whereas patchiness of DOC appeared to be

influenced by heterogeneity at landscape level, as illustrated by a similar semivariance among flow-connected and flow-unconnected sites.

4.3 Unique molecular signatures and seasonal differences

In total, FT-ICR MS detected 4,283 molecular formulae, of which 3,607 and 3,674 were present in summer and winter, respectively. No trend in the number of formulae were observed along the DWTT gradient in either season (supporting information Figure S2), with the number of formulae found in each sample ranging between 1,609 and 2,411 and between 1,572 and 2,380 in summer and winter, respectively. Molecular formulae classified as highly-unsaturated aliphatics dominated DOM in both summer (n=1958) and winter (n=1939), followed by formulae classified as polyphenols (n=759 and 803, respectively) and black carbon (n=491 and 688, respectively), while the remaining compound categories (peptides, saturated fatty acids, sugars and unsaturated aliphatics) contributed only 11.1 and 6.6% of the total number of molecular formulae in summer and winter, respectively (supporting information Figure S3). Neither the number of molecular formulae nor the summed relative intensity of these compound categories changed along the DWTT gradient (supporting information Figure S3). In both seasons, around 50% of all formulae were already present in the smallest headwaters within the Ybbs River network, whereas – when accumulating formulae in downstream direction – 90% of all formulae were detected after relatively short DWTT values of 241 and 253 minutes in summer and winter, respectively (Figure 3).

Of the 4,283 molecular formulae, 47.9% were found in less than half of the sites in summer and winter (supporting information Figure S4). We consider these as a population of rare formulae. On the other hand, a population of common formulae was detected in more than half of the sites

in summer and winter, and accounted for 35.5% of the total pool. 8.5% and 7.8% of all molecular formulae were season-specific, i.e. they were common in summer but not in winter and *vice versa*. In van Krevelen diagrams, common formulae populated the central region typical for carboxyl-rich alicyclic molecules (CRAM), while rare formulae populated the region typical for N-containing compounds and black carbon (supporting information Figure S5). Summer- and winter-specific populations clearly separated in van Krevelen diagrams with lignin- and protein-like formulae dominating in summer and tannin-like formulae dominating in winter (supporting information Figure S4). Average nominal mass was lower in summer- (456.2 Da) than in winter-specific populations (609.4 Da) (Welch T Test, $t=-18.508$, $p<0.01$). Average molecular C:N ratio was also lower for summer- (14.4) as compared to winter-specific (17.4) DOM populations (Welch T-Test, $t=-2.436$, $p<0.05$). Similarly, average NOSC was lower in summer- (-0.65) than in winter-specific populations (0.34) (Welch T-Test, $t=-41.014$, $p<0.01$) (supporting information Figure S4). The average relative contribution of all formulae in the summer- and winter-specific populations increased from 4.6 to 6.5% across the DWTT gradient in summer, but stayed almost stable at 7% in winter, respectively (supporting information Figure S4).

4.4 Compositional changes of DOM across the Ybbs River network

We investigated the compositional changes in DOM along the DWTT gradient using a combination of canonical correlation analysis, PLS modeling and direct correlation of relative molecular intensities with DWTT. DOM molecular composition was significantly related to DWTT in summer (canonical correlation, $r=0.85$, $p<0.01$) and winter (canonical correlation, $r=0.87$, $p<0.01$). Highly significant ($p<0.001$) PLS models explained 73% and 47% of the

variation in DWTT from the relative distribution of DOM formulae in the training and validation data, respectively. Interestingly, VIP scores, which are a measure of the importance of variables for the projection, were negatively ($r=-.32$, $p<0.001$) related to the nominal mass of the formulae (supporting information Figure S6). DOM compounds with VIP scores > 1.5 (i.e. their relative intensity is highly predictive of DWTT, $n=329$) accounted for 7.6% of all detected compounds. However, taken together, the relative peak intensity of these highly predictive compounds ranged between 14.2 and 20.9% in summer and between 13.3 and 18.3% in winter. This suggests that a small proportion of abundant and predominantly low-molecular mass DOM compounds can serve as markers for DWTT across the Ybbs River network, and this even at the scale of a few hours.

Correlating relative peak intensities with DWTT, we found that formulae with a positive relationship to DWTT (i.e., their relative peak intensity increased through the network) and those with a negative relationship were separated along the H:C axis in van Krevelen space in summer but not in winter (Figure 4). In summer, the distribution of correlation coefficients (ranging from -0.41 to 0.45) was significantly skewed from a normal distribution (Kolmogorov-Smirnov Test, $D=0.39$, $p<0.01$) with a clear mode of positive correlation coefficients and a second, less pronounced but clearly negative mode (2,201 formulae had positive relationship with DWTT, whereas 1,406 formulae had negative relationships; Figure 4). In contrast, in winter, correlation coefficients (ranging from -0.28 to 0.44) were unimodally distributed around zero. Formulae with smaller nominal masses tended to be negatively related to DWTT in summer whereas no such trend was apparent in winter (Figure 4).

4.5 Spatial convergence of DOM molecules

We estimated the rate of decrease of variance along the DWTT gradient to identify molecular populations that converge to the catchment-scale average. In a plot of absolute residual intensity against DWTT, a steeper reduction of the triangular distribution outlined by the pareto-optimal front indicates a faster convergence to the catchment-scale average (supporting information Figure S7). 43% of all formulae detected in summer and 53% of the formula detected in winter complied with the selection criteria indicating a convergence to the catchment mean peak intensity (i.e. minimum of 4 pareto-optimal points). For summer, we were able to identify two chemically distinct populations that converged differently; no such pattern was observed for winter (Figure 5). In summer, the rapidly converging population contained tannin-like compounds, whereas the more slowly converging DOM population contained lignin-like compounds, pointing towards a patchy distribution of sources of tannin-like compounds and a widespread distribution of sources of lignin-like compounds in summer.

4.6 DOM mass transfer

Restricting our analyses to molecular formulae that were present in all reaches (summer: $n=1,111$; winter: $n=1,175$), we found average $v_{f\text{ app}}$ ranging from -0.72 to 0.65 mm min^{-1} in summer, when its distribution was significantly skewed towards positive $v_{f\text{ app}}$ values (supporting information Figure S8). In winter, $v_{f\text{ app}}$ values varied less (-0.21 to 0.25 mm min^{-1}) and were normally distributed around zero (supporting information Figure S8). Relating average $v_{f\text{ app}}$ values to NOSC at compound level, we found a significant negative relationship in summer ($R^2=0.34$, $p < 0.01$) and a weak negative relationship in winter ($R^2=0.005$, $p=0.01$) (Figure 6). This reflects a generally higher mass transfer of oxygenated compounds, classified mainly as highly unsaturated aliphatics. Furthermore, $v_{f\text{ app}}$ was negatively related to molecular mass in

summer ($R^2=0.21$, $p<0.01$) and weakly positively related to molecular mass in winter ($R^2=0.006$, $p<0.01$). Network-average compound availability measured as average relative peak intensity, compound aromaticity and H:C ratios were not related to $\nu_{f\text{ app}}$ (supporting information Figure S9).

By weighing $\nu_{f\text{ app}}$ with the relative peak intensity of the respective compound and summing these up for each reach (only those compounds present in each reach), we found that at the network scale, intensity-weighted $\nu_{f\text{ app}}$ showed highest variation among headwater streams (supporting information Figure S10). While intensity-weighted $\nu_{f\text{ app}}$ values were consistently negative across all reaches in winter, 11 of our study reaches had negative intensity-weighted $\nu_{f\text{ app}}$ in summer. Except for one, these reaches were nested in one sub-catchment. Inspection of intensity-weighted distribution of NOSC across the Ybbs River network (Figure 6) revealed that this sub-catchment also comprised DOM compounds with higher NOSC compared to the other reaches.

5 Discussion

Our analyses revealed the complex and dynamic nature of DOM at the molecular level within an Alpine stream network. In terms of molecular richness, as the number of detected formulae, our findings are comparable to those from other freshwater environments (Hutchins et al., 2017; Ide et al., 2017; Jaffé et al., 2012; Kim et al., 2006; Mosher et al., 2015; Seitzinger et al., 2005). In contrast to the predictions of the River Continuum Concept (Vannote et al., 1980) and a recent work on headwater streams (Mosher et al., 2015), we did not find a decreasing trend in the number of DOM compounds with increasing travel time (supporting information Figure S2). In these studies, DOM is considered to be highly diverse in headwaters due to proximity to soil and detrital sources. Then, selective removal of compounds along downstream transport diminishes

its diversity. As a consequence, downstream diversity patterns are thus increasingly driven by accumulating tannin- or lignin compounds resistant to degradation (Ide et al., 2017). In the Ybbs River network, most of the DOM compounds were already present in headwater streams (Figure 3) and remained detectable with increasing DWTT, where only few previously undetected compounds were identified in addition. This is in line with the large pool of shared DOM compounds across different streams in other studies (Gonsior et al., 2016; Jaffé et al., 2012; Mosher et al., 2015; Riedel et al., 2016). In contrast to shared, likely terrigenous DOM, the addition of novel compounds seems to happen rarely. Such additional compounds may also be cycled too rapidly to be detected or analytically not distinguishable without separation of structural isomers. We conclude that compositional changes, in particular shifts in relative intensity rather than presence/absence patterns, may thus better reflect the actual DOM dynamics subject to processing and mixing-induced discontinuities inherent to stream networks (Benda et al., 2004) than simple measures of DOM diversity.

Our findings highlight differential turnover of DOM populations in terms of their relative contribution to the entire DOM pool, as they move with the streamwater through the Ybbs River network (Figure 4). These shifts were highly predictive of the time DOM had spent in the stream network and were pronounced in summer, when predominantly small molecules and molecules with low H:C ratios decreased in relative abundance, whereas lignin- and protein-like compounds tended to accumulate. In contrast, indifferent dynamics characterized the spatial distribution of DOM compounds in winter. This is striking given that DWTT only marginally differed between the two seasons (supporting information Figure S1) and highlights the importance of seasonal variation in DOM source material and biogeochemical processing. The seasonal segregation of DOM may reflect the varying contributions from fresh plant material and

stream microorganisms (including algae) in summer and degrading leaf litter in winter (i.e. lignin- and protein-like formulae dominating in summer and tannin-like formulae dominating in winter, supporting information Figure S4, Figure 4). This notion is also supported by lower masses and lower C:N ratios in summer as they are typical for algal exudates, for instance, compared to the more processed and aged vascular plant material in winter. Besides these distinct populations, we also identified an ubiquitous population similar to CRAM, which appears to be a common component of both freshwater and marine DOM (Mosher et al., 2015; Stubbins et al., 2010; Zark & Dittmar, 2018). Because we also detected CRAM among the smallest headwaters within the Ybbs River network, we speculate that these compounds largely originated from soils and thus may be an important component of the lateral carbon flux to the oceans (Hertkorn et al., 2006).

Given a DWTT of 29 h and 34 h at the catchment outflow during summer and winter baseflow, respectively, our results indicate that DOM encountered sufficient opportunities for biotic processing, photochemical degradation or sorption to microbial biofilms (Freeman & Lock, 1995) or mineral surfaces (Hunter et al., 2016). These time scales are well beyond the time scales (i.e., up to 1.8 h) deemed relevant for DOC removal in streams (Battin et al., 2003; Kaplan & Newbold, 1995). In-stream biotic processes involved in DOM removal may be particularly relevant during periods of extended baseflow with long residence times, weak terrestrial-aquatic linkages and copious benthic biofilm covering the streambed. Our measure of DWTT captures significant longitudinal changes in DOM composition (PLS modelling, Figure 4) and uptake (Figure 6) at baseflow, yet, it does not encapsulate important processes such as lateral water input, subsurface transient storage phenomena or exchanges between soil-, ground- and streamwater. Incorporating these sources, transport and exchange processes will require ground-

truthed estimates of residence time distribution at relevant spatial resolution, and thus remains a future research task.

How the “funneling” of the DOM, that is its collection from the terrestrial landscape *and* its processing under travel time-related constraints, contributes to the formation and downstream diagenesis of the complex fluvial DOM pool remains poorly understood (Casas-Ruiz et al., 2017; Creed et al., 2015). Our findings unravel emergent properties of a stream network as it literally “funnels” DOM from various sources from headwaters to the catchment outlet during baseflow in summer and winter. Empirical semivariograms showed the spatial extent of patchiness in DOC concentration and electrical conductivity in the Ybbs River network on the order of 10-20 km. Spatial statistical analyses tailored to stream networks are powerful tools to understand the distribution and spatial dynamics of solutes (McGuire et al., 2014; Ver Hoef et al., 2014). However, extension of such analyses to account for the molecular complexity of DOM is challenging, given the relative nature of mass spectrometry data and the loss of resolution with dimensionality reduction of multivariate datasets. The symmetric convergence of streamwater DOC concentration to the catchment-level average suggests hydrologic averaging as a major driver of DOC biogeochemistry at the scale of the Ybbs River network. Similar homogenization of various solutes, including DOC, from stream networks has been reported earlier (Abbott et al., 2017; McGuire et al., 2014; Temnerud et al., 2007). For DOM, the symmetrical convergence at the landscape scale has been linked to hydrological mixing and a shift in dominance from terrestrial-aquatic connectivity in headwaters to in-stream production in larger streams (Creed et al., 2015). The relative spatial isolation of headwaters at landscape level and their tight coupling with the terrestrial milieu may underlie the chemical heterogeneity of DOM among these streams. This is comparable to the elevated dissimilarity of microbial communities among

headwater streams as previously reported from the Ybbs River network (Besemer et al., 2013). We suggest that, in the Ybbs River network, hydrological mixing at confluences, as reflected by streamwater electrical conductivity, explains a major part of the convergence of DOC concentration. Yet, in contrast to streamwater electrical conductivity, average DOC concentration decreased below the catchment-level average indicating net carbon removal. However, we did not find evidence for homogenization of DOM at the level of compound categories, such as the expected shift from aromatic to aliphatic compounds as autochthonous DOM increases with increasing stream order (Creed et al., 2015). The absence of homogenization at the molecular level may be related to simultaneous transformation processes or methodological limitations related to the relative nature of the FT-ICR MS approach. However, the convergence of DOM variability would also be expected to be most pronounced in large fluvial networks and the Ybbs River network may reflect the importance of connectivity to terrestrial source material in a 5th-order stream. The observed compositional turnover of DOM suggests shifts in sources to play an important role. In fact, our analytic approach allowed us to explore the rate of DOM convergence at compound level and thus to assess the spatial distribution of potential DOM sources within the Ybbs River network. Abbott et al. (2017) showed that the reduction of spatial variance across flow-connected sites in stream networks is related to the patch size of sources and sinks in the landscape. Accordingly, widely distributed and large source patches would result in a relatively slow convergence to the catchment-level average concentration of any given solute. In contrast, point sources result in a rapid convergence. Strikingly, we found two distinct molecular populations with fast and slow convergence rates in summer whereas in winter molecular formulae exhibited predominantly a slow convergence (Figure 5). This points to differences in source distribution among DOM

fractions in summer, but whether this is related to source-patch heterogeneity or patchiness of in-stream biogeochemical processes (at “hotspots”) remains to be explored. Source-patch heterogeneity of freshly produced, algal-derived DOM may be related to light availability, which may locally differ in summer depending on shading by riparian vegetation or landscape exposition. In winter, DOM sources appear more uniformly and widely distributed, which may reflect reduced in-stream processing at low water temperatures or widely distributed leaf-litter as a source of DOM.

The apparent mass transfer coefficient of DOM compounds, $v_{f\text{app}}$, translates to the vertical uptake velocity and determines their ultimate fate at the stream network scale (Creed et al., 2015). The reach-scale mass transfer coefficients of individual DOM compounds reported here (Figure 6) were very similar to values obtained from flume experiments (Singer et al., 2010) and uptake velocities of bulk DOC (Mineau et al., 2016). Bioavailability has been previously linked to DOM properties (Guillemette & del Giorgio, 2011; Riedel et al., 2016; Seitzinger et al., 2005) such as molecular size (Kaplan & Bott, 1983), H:C ratio (Sun et al., 1997), aromaticity (Koch & Dittmar, 2006) and the oxidative state, as it should be thermodynamically favorable to oxidize DOM as NOSC increases (LaRowe & Van Cappellen, 2011). Indeed, we found a relationship between the oxidative state and $v_{f\text{app}}$ in the Ybbs River network, in line with those reported from flume experiments (Singer et al., 2010) and short-term bio-incubation studies (Kim et al., 2006; Seidel et al., 2015). This may affect landscape-scale pattern of DOM processing, as DOM of varying bioavailability from upstream sources propagates through the network.

6 Conclusions

In conclusion, we show that DWTT captures important spatial and temporal constraints on the molecular composition of DOM in a fluvial network. We found that mixing at confluences alongside continuous DOM processing including removal as well as production are important drivers of spatial DOM turnover and suggest that accounting for the molecular complexity of DOM is critical to more mechanistically understand the various processes that act in concert upon DOM in fluvial networks. Pronounced seasonality in the distribution of sources of DOM further imprints on the molecular distribution of DOM, yet spatial DOM turnover in winter was limited, likely because of constrained microbial processing at low water temperatures and reduced algal production at low light availability. Finally, molecular properties of DOM such as the oxidative state of DOM, which bears signatures of landscape-scale patterns, underlies the apparent uptake velocity of DOM compounds. It is pivotal to better understand the timescales and spatial processes that contribute to the formation and diagenesis of the DOM pool as water moves through the landscape since this is directly linked to the greenhouse gas emission potential of streams and rivers.

Acknowledgments and Data

Raw data will be made publicly available on Figshare upon publication. The data is already accessible for reviewers under this private link: <https://figshare.com/s/1edbd38e75a0e8132593> We thank Beate Eichelberger and Gertraud Stenizcka, Katharina Besemer and numerous other colleagues from the WasserCluster Lunz for help in the field and laboratory. Funding came from the Austrian Science Foundation (START Y420-B17) to T.J.B.

References

- Abbott, B. W., Gruau, G., Zarnetske, J. P., Moatar, F., Barbe, L., Thomas, Z., et al. (2017). Unexpected spatial stability of water chemistry in headwater stream networks. *Ecology Letters*, 21(2), 296-308.
- Aiken, G. R., Hsu-Kim, H., & Ryan, J. N. (2011). Influence of Dissolved Organic Matter on the Environmental Fate of Metals, Nanoparticles, and Colloids. *Environmental Science & Technology*, 45(8), 3196-3201.
- Barnes, R. T., Butman, D. E., Wilson, H. F., & Raymond, P. A. (2018). Riverine Export of Aged Carbon Driven by Flow Path Depth and Residence Time. *Environ Sci Technol*, 52(3), 1028-1035.
- Battin, T. J., Kaplan, L. A., Findlay, S., Hopkinson, C. S., Marti, E., Packman, A. I., et al. (2008). Biophysical controls on organic carbon fluxes in fluvial networks. *Nature Geoscience*, 1(2), 95-100.
- Battin, T. J., Kaplan, L. A., Newbold, J. D., & Hendricks, S. P. (2003). A mixing model analysis of stream solute dynamics and the contribution of a hyporheic zone to ecosystem function. *Freshwater Biology*, 48(6), 995-1014.
- Benda, L., Poff, N. L., Miller, D., Dunne, T., Reeves, G., Pess, G., & Pollock, M. (2004). The Network Dynamics Hypothesis: How Channel Networks Structure Riverine Habitats. *BioScience*, 54(5), 413-427.
- Berggren, M., & del Giorgio, P. A. (2015). Distinct patterns of microbial metabolism associated to riverine dissolved organic carbon of different source and quality. *Journal of Geophysical Research: Biogeosciences*, 120(6), 989-999.
- Bernhardt, E. S., Heffernan, J. B., Grimm, N. B., Stanley, E. H., Harvey, J. W., Arroita, M., et al. (2017). The metabolic regimes of flowing waters. *Limnology and Oceanography*, 63(S1), 99-118.
- Bertuzzo, E., Helton, A. M., Hall, R. O., & Battin, T. J. (2017). Scaling of dissolved organic carbon removal in river networks. *Advances in Water Resources*, 110, 136-146.
- Besemer, K., Singer, G., Quince, C., Bertuzzo, E., Sloan, W., & Battin, T. J. (2013). Headwaters are critical reservoirs of microbial diversity for fluvial networks. *Proceedings of the Royal Society B-Biological Sciences*, 280(1771).
- Casas-Ruiz, J. P., Catalán, N., Gómez-Gener, L., von Schiller, D., Obrador, B., Kothawala, D. N., et al. (2017). A tale of pipes and reactors: Controls on the in-stream dynamics of dissolved organic matter in rivers. *Limnology and Oceanography*, 62(S1), 85-94.
- Catalán, N., Marcé, R., Kothawala, D. N., & Tranvik, L. J. (2016). Organic carbon decomposition rates controlled by water retention time across inland waters. *Nature Geoscience*, 9, 501.
- Ceola, S., Bertuzzo, E., Singer, G., Battin, T. J., Montanari, A., & Rinaldo, A. (2014). Hydrologic controls on basin-scale distribution of benthic invertebrates. *Water Resources Research*, 50(4), 2903-2920.
- Creed, I. F., McKnight, D. M., Pellerin, B. A., Green, M. B., Bergamaschi, B. A., Aiken, G. R., et al. (2015). The river as a chemostat: fresh perspectives on dissolved organic matter flowing down the river continuum. *Canadian Journal of Fisheries and Aquatic Sciences*, 72(8), 1272-1285.
- Dittmar, T., Koch, B., Hertkorn, N., & Kattner, G. (2008). A simple and efficient method for the solid-phase extraction of dissolved organic matter (SPE-DOM) from seawater. *Limnology and Oceanography-Methods*, 6, 230-235.
- Eriksson, L., Johansson, E., Kettaneh-Wold, N., Trygg, J., Wikström, C., & Wold, S. (2006). *Multi- and Megavariate Data Analysis: Part I Basic Principles and Applications* (2 ed.). Umeå: Umetrics AB.

- 637 Ford, T. E., Ford, S. A., Lock, M. A., & Naiman, R. J. (1990). Dissolved organic carbon concentrations and fluxes
638 along the Moisie River, Quebec. *Freshwater Biology*, 24(1), 35-42.
- 639 Freeman, C., & Lock, M. A. (1995). The biofilm polysaccharide matrix: A buffer against changing organic substrate
640 supply? *Limnology and Oceanography*, 40(2), 273-278.
- 641 Gonsior, M., Peake, B. M., Cooper, W. T., Podgorski, D., D'Andrilli, J., & Cooper, W. J. (2009). Photochemically
642 Induced Changes in Dissolved Organic Matter Identified by Ultrahigh Resolution Fourier Transform Ion
643 Cyclotron Resonance Mass Spectrometry. *Environmental Science & Technology*, 43(3), 698-703.
- 644 Gonsior, M., Valle, J., Schmitt-Kopplin, P., Hertkorn, N., Bastviken, D., Luek, J., et al. (2016). Chemodiversity of
645 dissolved organic matter in the Amazon Basin. *Biogeosciences*, 13(14), 4279-4290.
- 646 Guillemette, F., & del Giorgio, P. A. (2011). Reconstructing the various facets of dissolved organic carbon
647 bioavailability in freshwater ecosystems. *Limnology and Oceanography*, 56(2), 734-748.
- 648 Guillemette, F., & del Giorgio, P. A. (2012). Simultaneous consumption and production of fluorescent dissolved
649 organic matter by lake bacterioplankton. *Environmental Microbiology*, 14(6), 1432-1443.
- 650 Hall, R. O., & Meyer, J. L. (1998). The trophic significance of bacteria in a detritus-based stream food web.
651 *Ecology*, 79(6).
- 652 Hertkorn, N., Benner, R., Frommberger, M., Schmitt-Kopplin, P., Witt, M., Kaiser, K., et al. (2006).
653 Characterization of a major refractory component of marine dissolved organic matter. *Geochimica et*
654 *Cosmochimica Acta*, 70(12), 2990-3010.
- 655 Hrachowitz, M., Benettin, P., van Breukelen, B. M., Fovet, O., Howden, N. J. K., Ruiz, L., et al. (2016). Transit
656 times—the link between hydrology and water quality at the catchment scale. *Wiley Interdisciplinary*
657 *Reviews: Water*, 3(5), 629-657.
- 658 Hunter, W. R., Niederdorfer, R., Gernand, A., Veuger, B., Prommer, J., Mooshammer, M., et al. (2016). Metabolism
659 of mineral-sorbed organic matter and microbial lifestyles in fluvial ecosystems. *Geophysical Research*
660 *Letters*, 43(4).
- 661 Hutchins, R. H. S., Aukes, P., Schiff, S. L., Dittmar, T., Prairie, Y. T., & Del Giorgio, P. A. (2017). The Optical,
662 Chemical, and Molecular Dissolved Organic Matter Succession Along a Boreal Soil-Stream-River
663 Continuum. *Journal of Geophysical Research: Biogeosciences*, 122(11), 2892-2908.
- 664 Ide, J. i., Ohashi, M., Takahashi, K., Sugiyama, Y., Piirainen, S., Kortelainen, P., et al. (2017). Spatial variations in
665 the molecular diversity of dissolved organic matter in water moving through a boreal forest in eastern
666 Finland. *Scientific Reports*, 7, 42102.
- 667 Jaffé, R., Yamashita, Y., Maie, N., Cooper, W. T., Dittmar, T., Dodds, W. K., et al. (2012). Dissolved Organic
668 Matter in Headwater Streams: Compositional Variability across Climatic Regions of North America.
669 *Geochimica et Cosmochimica Acta*, 94, 95-108.
- 670 Kaplan, L. A., & Bott, T. L. (1983). Microbial heterotrophic utilization of dissolved organic matter in a piedmont
671 stream. *Freshwater Biology*, 13(4), 363-377.
- 672 Kaplan, L. A., & Newbold, J. D. (1995). Measurement of streamwater biodegradable dissolved organic carbon with
673 a plug-flow bioreactor. *Water Research*, 29(12), 2696-2706.
- 674 Kayler, Z. E., Premke, K., Gessler, A., Gessner, M. O., Griebler, C., Hilt, S., et al. (2019). Integrating Aquatic and
675 Terrestrial Perspectives to Improve Insights Into Organic Matter Cycling at the Landscape Scale. *Frontiers*
676 *in Earth Science*, 7(127).

- 677 Kellerman, A. M., Dittmar, T., Kothawala, D. N., & Tranvik, L. J. (2014). Chemodiversity of dissolved organic
678 matter in lakes driven by climate and hydrology. *Nature Communications*, 5:3804
- 679 Kim, S., Kaplan, L. A., & Hatcher, P. G. (2006). Biodegradable dissolved organic matter in a temperate and a
680 tropical stream determined from ultra-high resolution mass spectrometry. *Limnology and Oceanography*,
681 51(2), 1054-1063.
- 682 Koch, B., & Dittmar, T. (2006). From mass to structure: An aromaticity index for high-resolution mass data of
683 natural organic matter. *Rapid communications in mass spectrometry*, 20(5), 926-932.
- 684 LaRowe, D. E., & Van Cappellen, P. (2011). Degradation of natural organic matter: A thermodynamic analysis.
685 *Geochimica et Cosmochimica Acta*, 75(8), 2030-2042.
- 686 Leopold, L., & Maddock, T. (1953). The hydraulic geometry of stream channels and some physiographic
687 implications. *Geological Survey Professional Paper*, 252.
- 688 Lu, Y., Li, X., Mesfioui, R., Bauer, J. E., Chambers, R. M., Canuel, E. A., & Hatcher, P. G. (2015). Use of ESI-
689 FTICR-MS to Characterize Dissolved Organic Matter in Headwater Streams Draining Forest-Dominated
690 and Pasture-Dominated Watersheds. *PLOS ONE*, 10(12), e0145639.
- 691 McGuire, K. J., Torgersen, C. E., Likens, G. E., Buso, D. C., Lowe, W. H., & Bailey, S. W. (2014). Network
692 analysis reveals multiscale controls on streamwater chemistry. *Proceedings of the National Academy of*
693 *Sciences*, 111(19), 7030-7035.
- 694 Mineau, M. M., Wollheim, W. M., Buffam, I., Findlay, S. E. G., Hall Jr., R. O., Hotchkiss, E. R., et al. (2016).
695 Dissolved organic carbon uptake in streams: A review and assessment of reach-scale measurements.
696 *Journal of Geophysical Research: Biogeosciences*, 121(8), 2019-2029.
- 697 Mosher, J. J., Kaplan, L. A., Podgorski, D. C., McKenna, A. M., & Marshall, A. G. (2015). Longitudinal shifts in
698 dissolved organic matter chemogeography and chemodiversity within headwater streams: a river continuum
699 reprise. *Biogeochemistry*, 124(1), 371-385.
- 700 Mostovaya, A., Hawkes, J. A., Koehler, B., Dittmar, T., & Tranvik, L. J. (2017). Emergence of the Reactivity
701 Continuum of Organic Matter from Kinetics of a Multitude of Individual Molecular Constituents.
702 *Environmental Science & Technology*, 51(20), 11571-11579.
- 703 Oksanen, J., Blanchet, F. G., Kindt, R., Legendre, P., Minchin, P. R., O'Hara, R. B., et al. (2013). vegan:
704 Community Ecology Package. R package version 2.0-9.
- 705 Regnier, P., Friedlingstein, P., Ciais, P., Mackenzie, F. T., Gruber, N., Janssens, I. A., et al. (2013). Anthropogenic
706 perturbation of the carbon fluxes from land to ocean. *Nature Geoscience*, 6, 597.
- 707 Riedel, T., Biester, H., & Dittmar, T. (2012). Molecular Fractionation of Dissolved Organic Matter with Metal Salts.
708 *Environmental Science & Technology*, 46(8), 4419-4426.
- 709 Riedel, T., Zark, M., Vähätalo, A. V., Niggemann, J., Spencer, R. G. M., Hernes, P. J., & Dittmar, T. (2016).
710 Molecular Signatures of Biogeochemical Transformations in Dissolved Organic Matter from Ten World
711 Rivers. *Frontiers in Earth Science*, 4(85).
- 712 Rigby, R. A., & Stasinopoulos, D. M. (2005). Generalized additive models for location, scale and shape. *Journal of*
713 *the Royal Statistical Society: Series C (Applied Statistics)*, 54(3), 507-554.
- 714 Seidel, M., Yager, P. L., Ward, N. D., Carpenter, E. J., Gomes, H. R., Krusche, A. V., et al. (2015). Molecular-level
715 changes of dissolved organic matter along the Amazon River-to-ocean continuum. *Marine Chemistry*, 177,
716 218-231.

- Seitzinger, S. P., Hartnett, H., Lauck, R., Mazurek, M., Minegishi, T., Spyres, G., & Styles, R. (2005). Molecular-level chemical characterization and bioavailability of dissolved organic matter in stream water using electrospray-ionization mass spectrometry. *Limnology and Oceanography*, 50(1), 1-12.
- Singer, G., Besemer, K., Schmitt-Kopplin, P., Hodl, I., & Battin, T. J. (2010). Physical heterogeneity increases biofilm resource use and its molecular diversity in stream mesocosms. *PLOS ONE*, 5(3), e9988.
- Singer, G., Fasching, C., Wilhelm, L., Niggemann, J., Steier, P., Dittmar, T., & Battin, T. J. (2012). Biogeochemically diverse organic matter in Alpine glaciers and its downstream fate. *Nature Geoscience*, 5(10), 710-714.
- Sleighter, R. L., Cory, R. M., Kaplan, L. A., Abdulla, H. A. N., & Hatcher, P. G. (2014). A coupled geochemical and biogeochemical approach to characterize the bioreactivity of dissolved organic matter from a headwater stream. *Journal of Geophysical Research: Biogeosciences*, 119(8), 1520-1537.
- Stubbins, A., Spencer, R. G. M., Chen, H., Hatcher, P. G., Mopper, K., Hernes, P. J., et al. (2010). Illuminated darkness: Molecular signatures of Congo River dissolved organic matter and its photochemical alteration as revealed by ultrahigh precision mass spectrometry. *Limnology and Oceanography*, 55(4), 1467-1477.
- Sun, L., Perdue, E. M., Meyer, J. L., & Weis, J. (1997). Use of elemental composition to predict bioavailability of dissolved organic matter in a Georgia river. *Limnology and Oceanography*, 42(4), 714-721.
- Temnerud, J., Seibert, J., Jansson, M., & Bishop, K. (2007). Spatial variation in discharge and concentrations of organic carbon in a catchment network of boreal streams in northern Sweden. *Journal of Hydrology*, 342(1), 72-87.
- Vannote, R. L., Minshall, G. W., W., C. K., Sedell, J. R., & Cushing, C. E. (1980). The River Continuum Concept. *Canadian Journal of Fisheries and Aquatic Sciences*, 37, 130-137.
- Ver Hoef, J., Peterson, E., Clifford, D., & Shah, R. (2014). SSN: An R Package for Spatial Statistical Modeling on Stream Networks. 2014, 56(3), 45.
- Zark, M., & Dittmar, T. (2018). Universal molecular structures in natural dissolved organic matter. *Nature Communications*, 9(1), 3178.

Figure 1. The Ybbs River network color coded according to discharge weighted average travel time (DWTT) estimated from hydraulic scaling relationships at summer baseflow. Sampling locations (red circles, n=148) were nested around major confluences to maximize reach length. Filled circles indicate that both seasons were sampled.

Figure 2 z-scaled DOC concentration (red for summer, blue for winter) and stream water electrical conductivity (grey) in summer (A) and winter (B). The solid lines show the mean and dotted lines show the 10% and 90% centiles of Generalized Additive Models for Location, Scale and Shape (GAMLSS) model fits. Both DOC concentration and electrical conductivity converged symmetrically to the catchment average, indicative of conservative mixing being an important driver of spatial patterns of streamwater DOC. In both seasons, mean DOC showed a negative trend, reflecting net DOC removal. Torgegrams show the spatial autocorrelation structure of DOC concentration (colored) and stream water conductivity (grey) for summer (C) and winter (D). Normalized semivariance increased as distance between neighboring sites increased, indicative of spatial patchiness. Semivariance of DOC and conductivity asymptotes at approx. 10 – 20 km separation distance in both seasons. Electrical conductivity showed a clear

separation between flow-connected and flow-unconnected separation distances, with higher semivariance between flow-connected sites. Such a separation was not evident for DOC concentration, indicating that downstream flow exerted a dominant control on electrical conductivity but not on DOC concentration.

Figure 3 The number of accumulated novel compounds saturated rapidly as water moved through the Ybbs River network. Vertical lines indicate DWTT at which 90% of all molecular formulae were detected in summer (red) and winter (blue), respectively. Note that a large fraction of DOM diversity was already present in the uppermost headwater streams.

Figure 4 Van Krevelen diagrams of molecular formulae in the Ybbs River network for summer (A) and winter (B) color-coded according to the correlation coefficient (r) of relative peak intensity with DWTT. The density contours (solid lines) include 75%, 50% and 25% of DOM formulae with positive (red) and negative (blue) correlations with DWTT. The distributions of r with comparison to a random distribution around zero are given above, the distributions of r as a function of nominal mass are shown below the respective van Krevelen diagrams.

Figure 5 Van Krevelen diagrams color-coded according to the rate of convergence in the network for summer (A) and winter (B). Darker colors indicate a faster, lighter colors a relatively slow convergence to the catchment average. Fast convergence gradients indicate distinct (small-scale) point sources of the respective compounds in the headwaters, whereas slow convergence indicates conservative mixing or large-scale sources throughout the network.

Figure 6 Shown are Van Krevelen plots with molecular formulae color coded according to the network-average estimates of $v_{f\ app}$ in summer (A) and winter (B). $v_{f\ app}$ versus the nominal oxidative state of carbon (NOSC) for summer (C) and winter (D), color-coded for different DOM categories. The solid line represents the linear model fit, dashed lines represent the 95% prediction intervals. Panels E and F show the spatial distribution of intensity-weighted NOSC as a measure of the average oxidative state of the DOM pool in summer and winter, respectively. Note the spatial variation in intensity-weighted NOSC at subcatchment scale (particularly in panel E).

Figure 1.

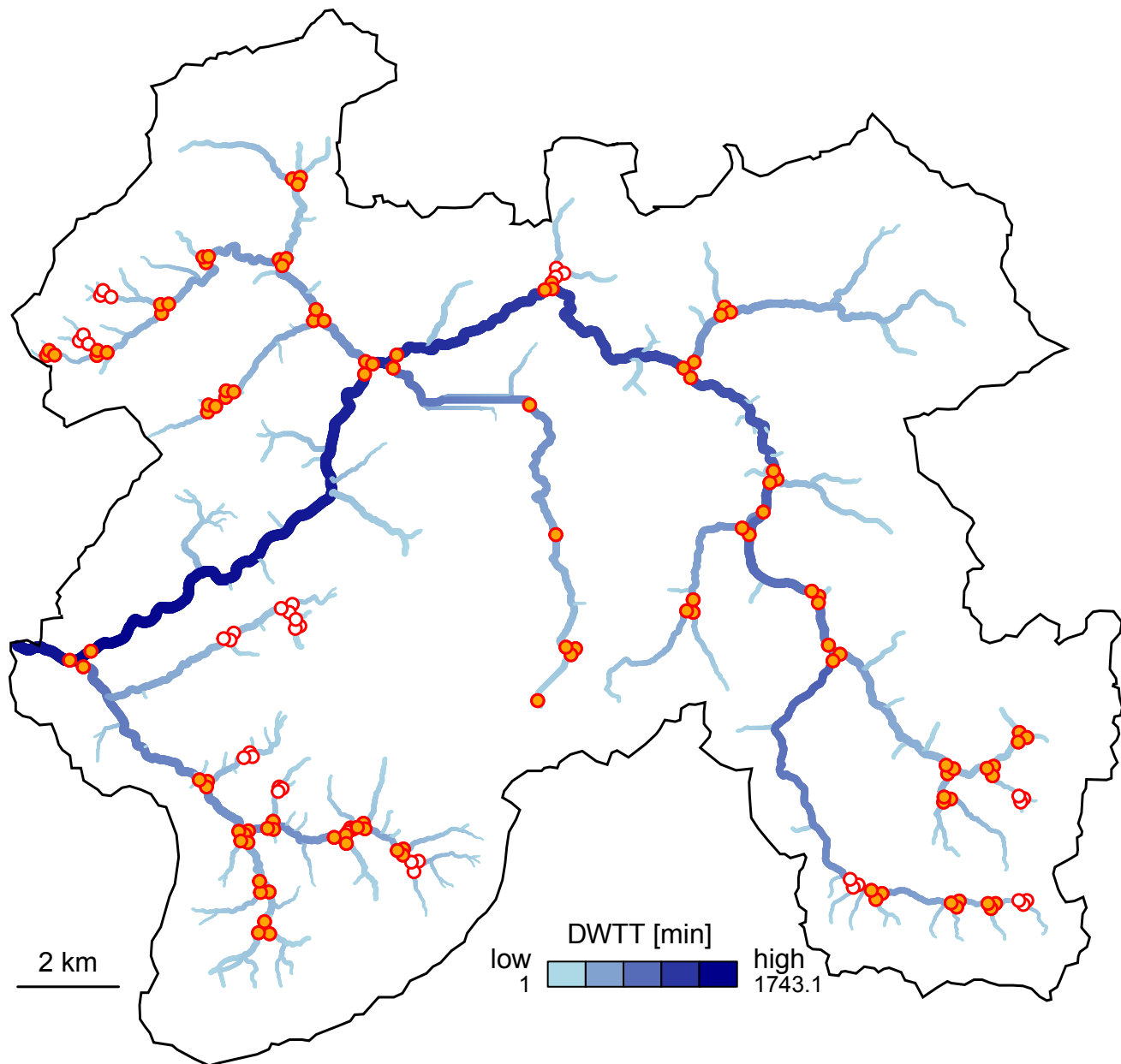


Figure 2.

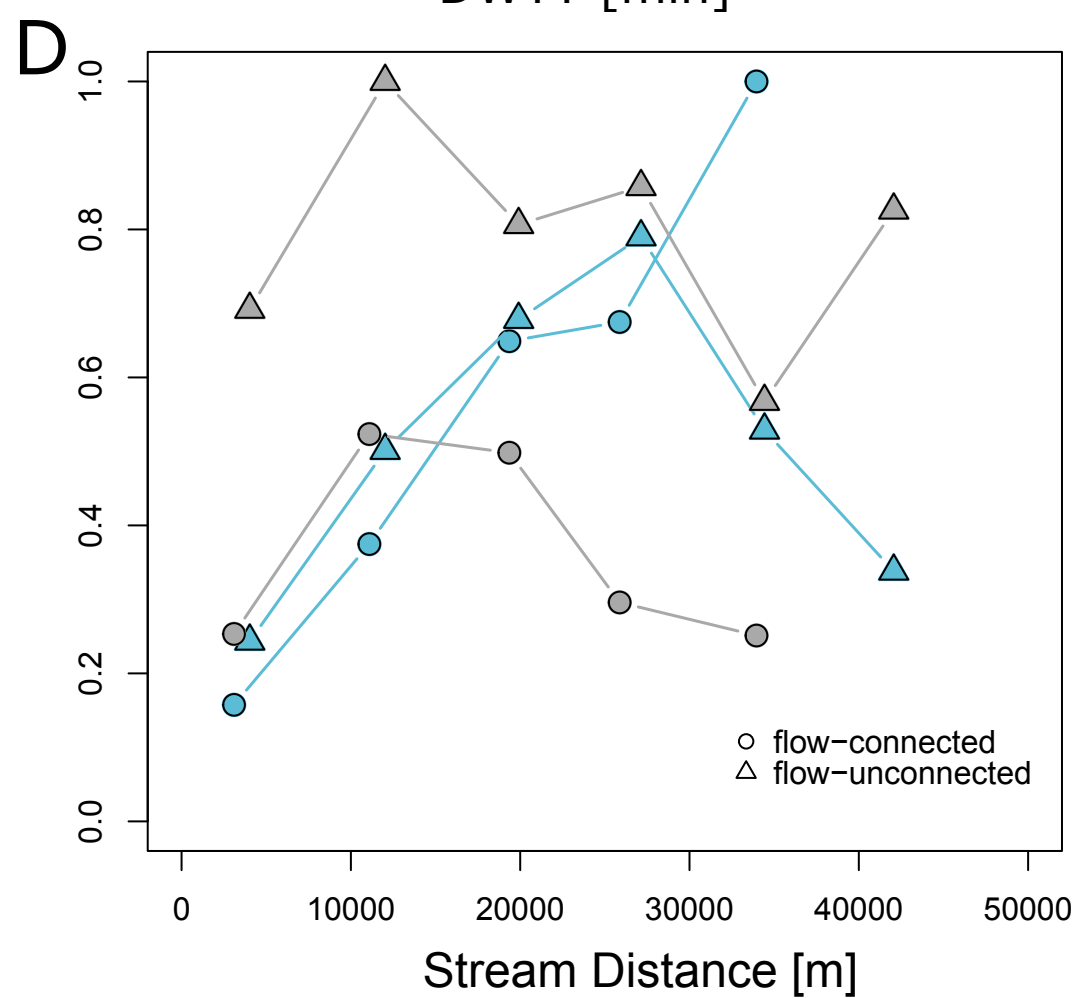
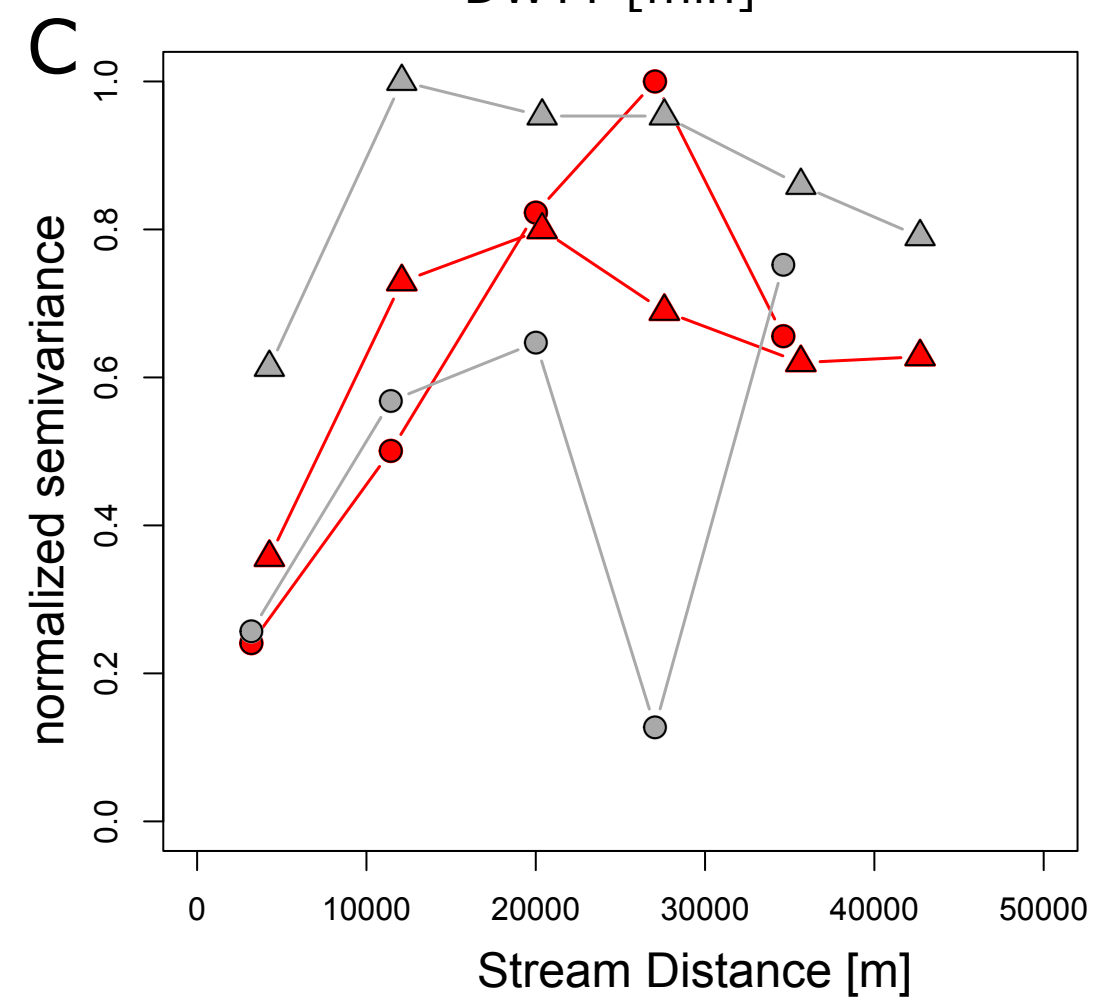
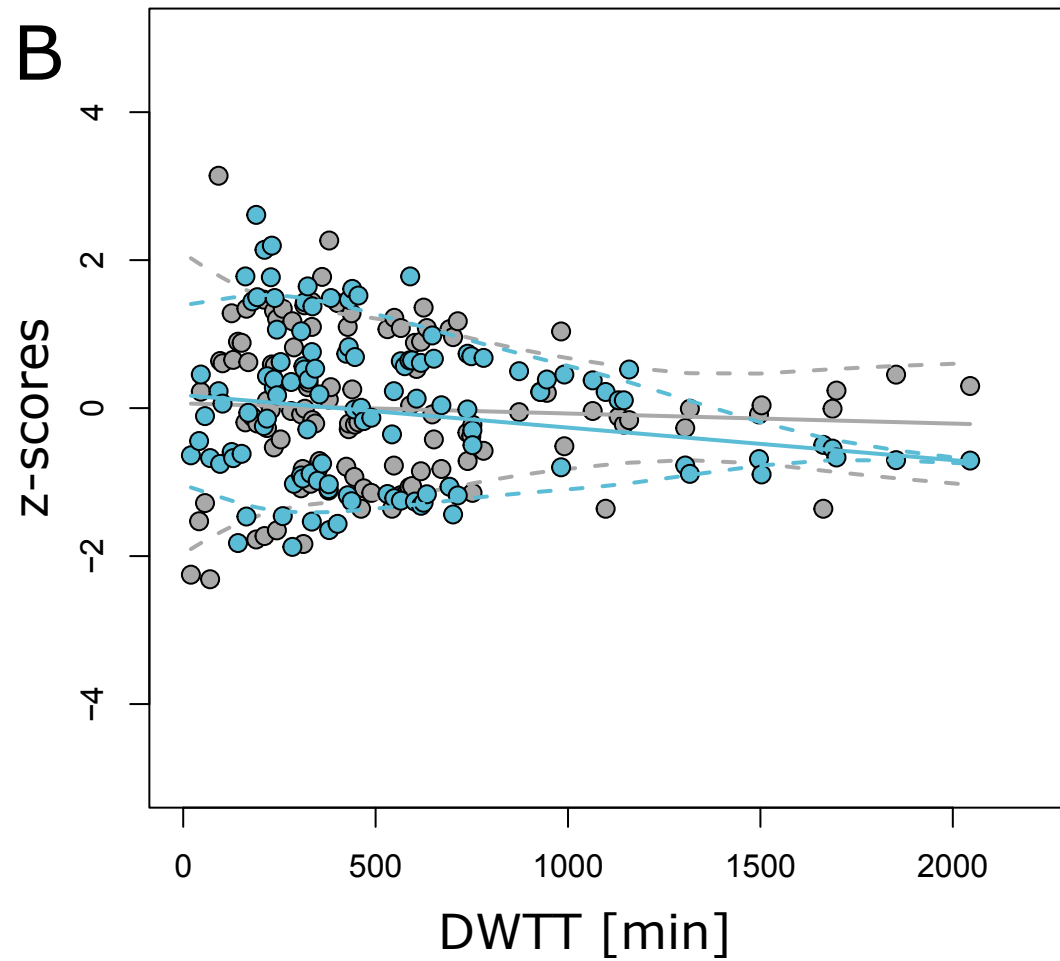
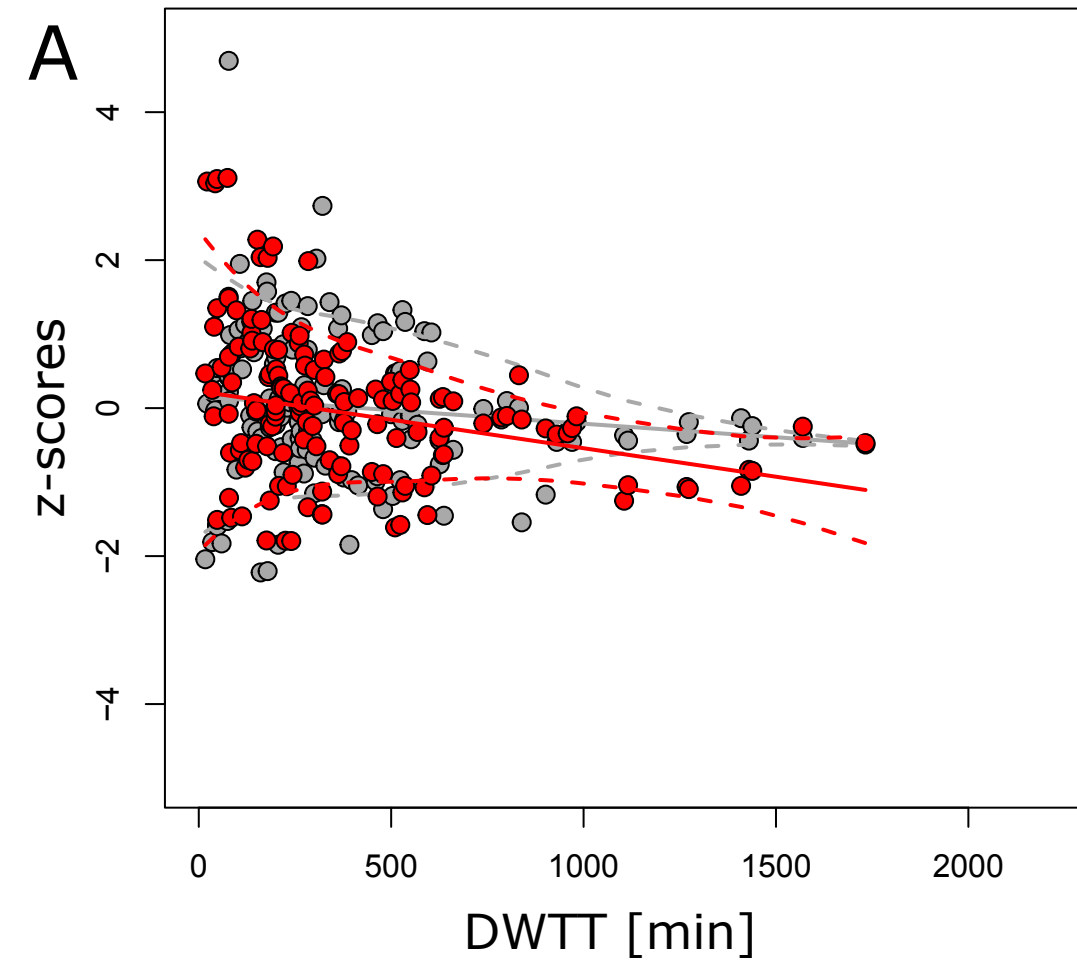


Figure 3.

cumulative number of formulae

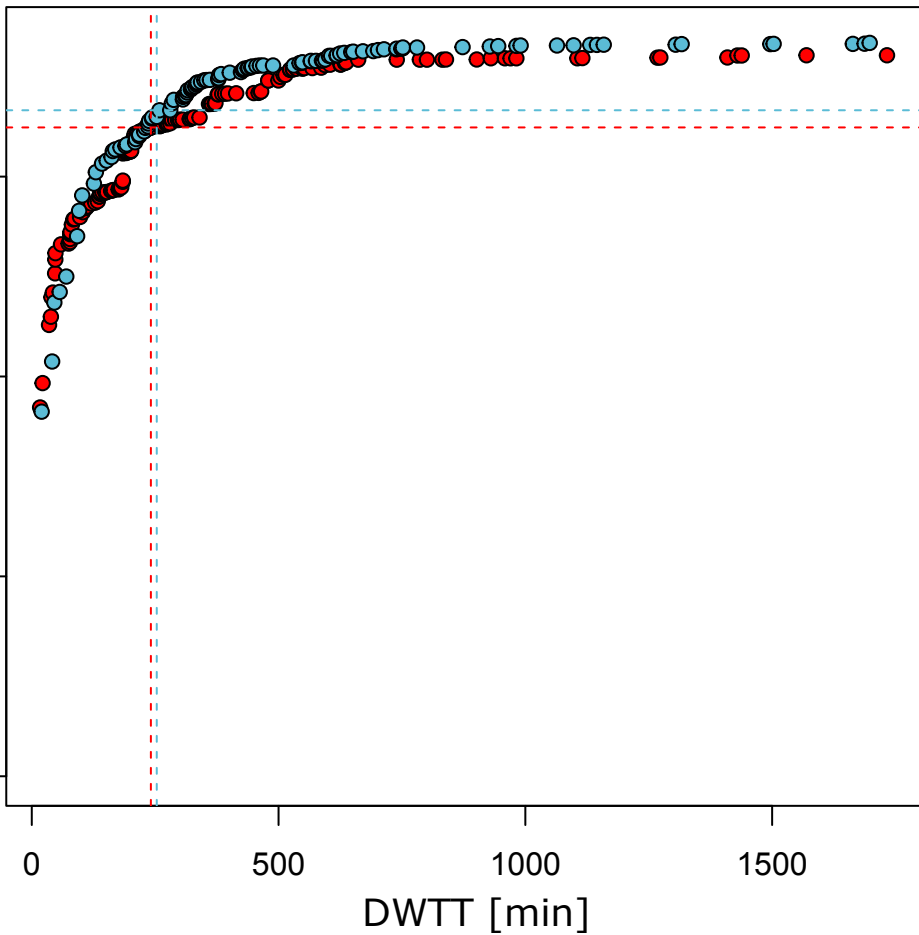


Figure 4.

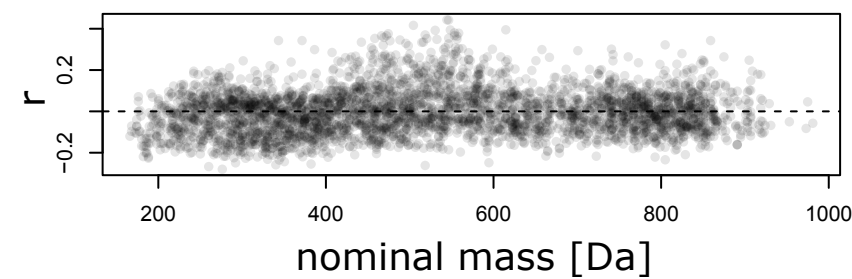
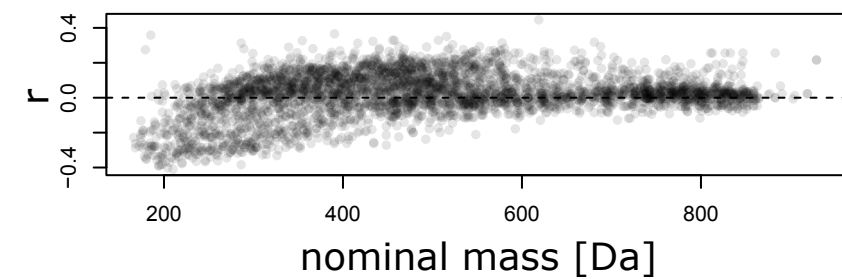
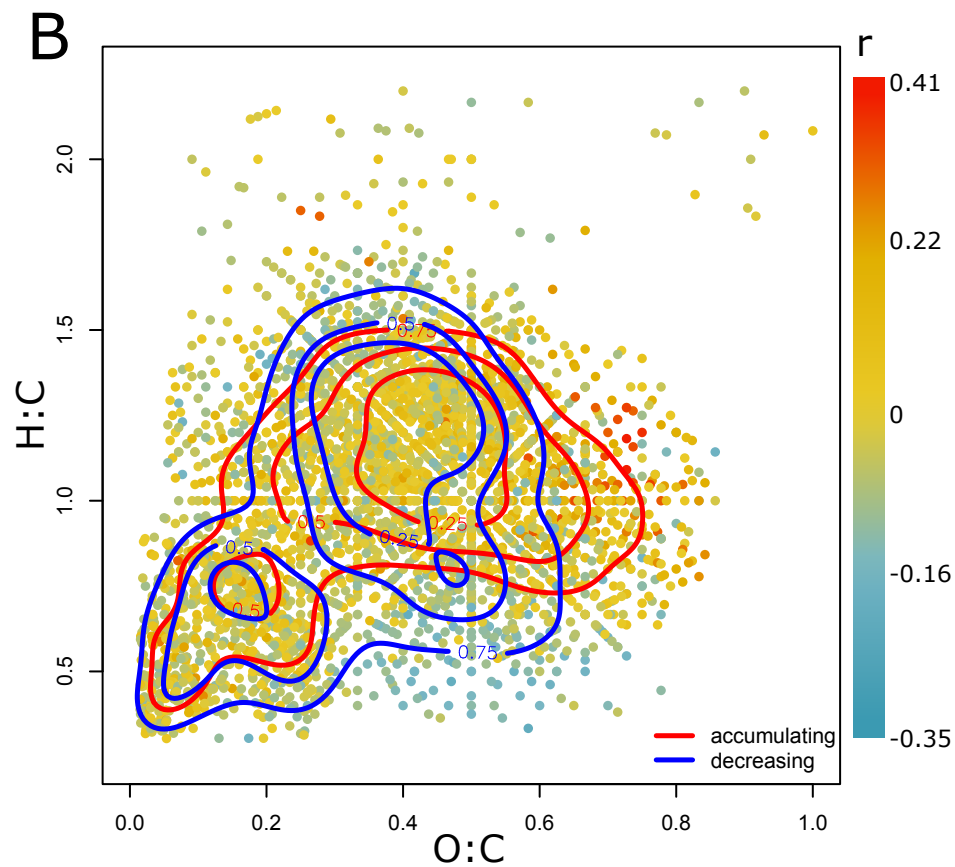
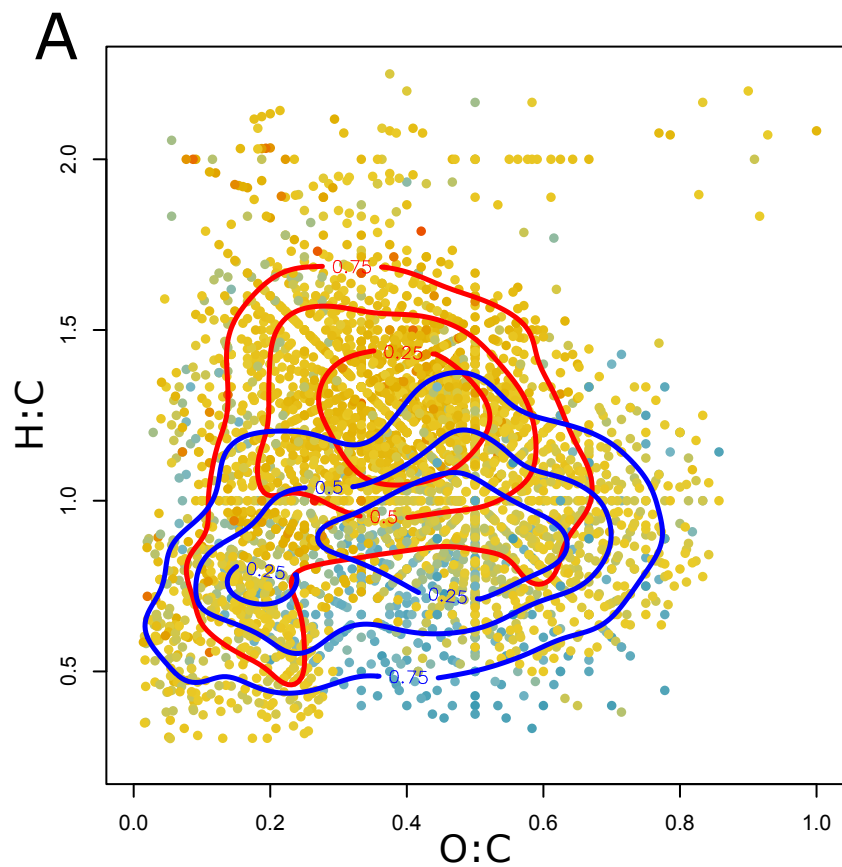
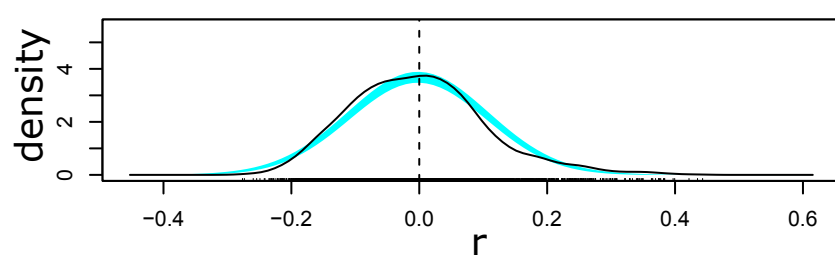
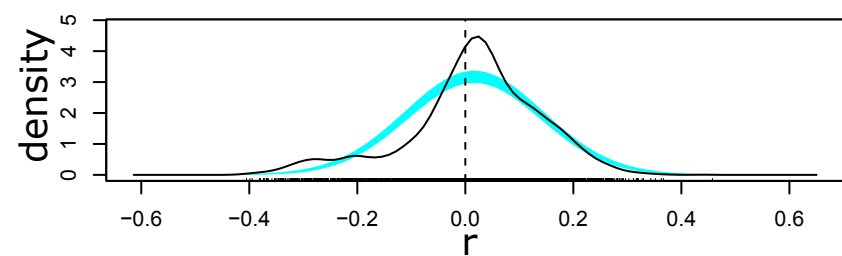


Figure 5.

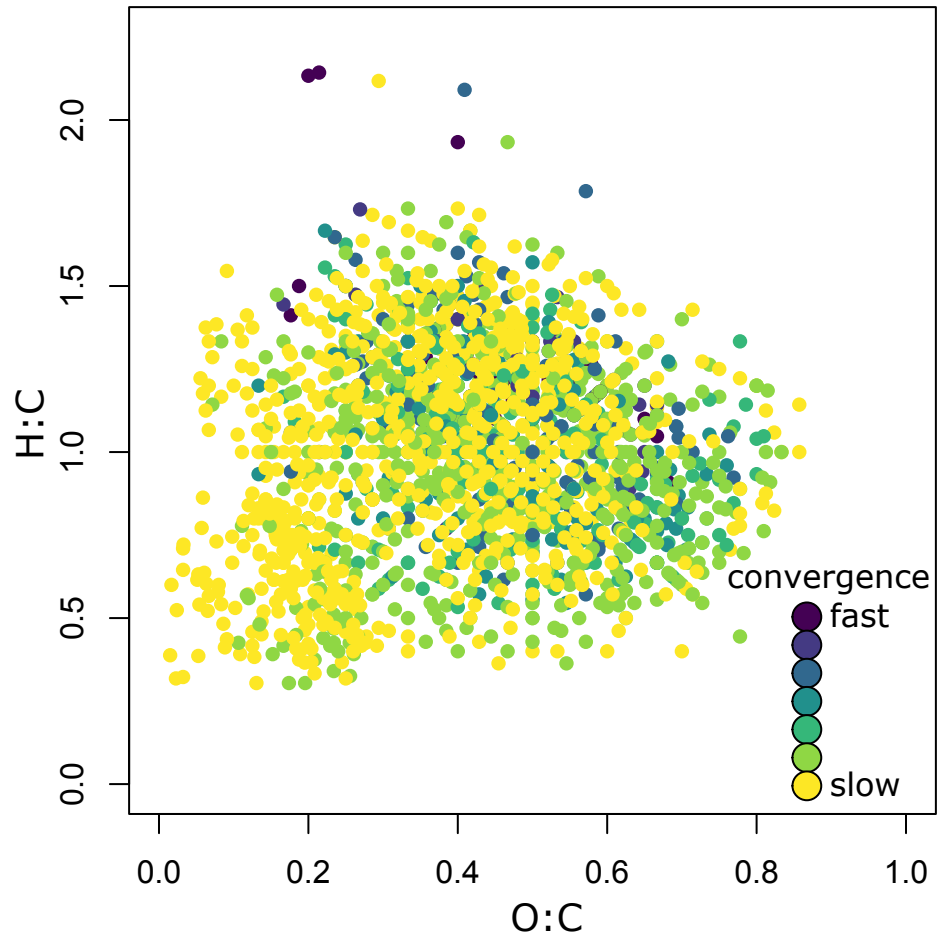
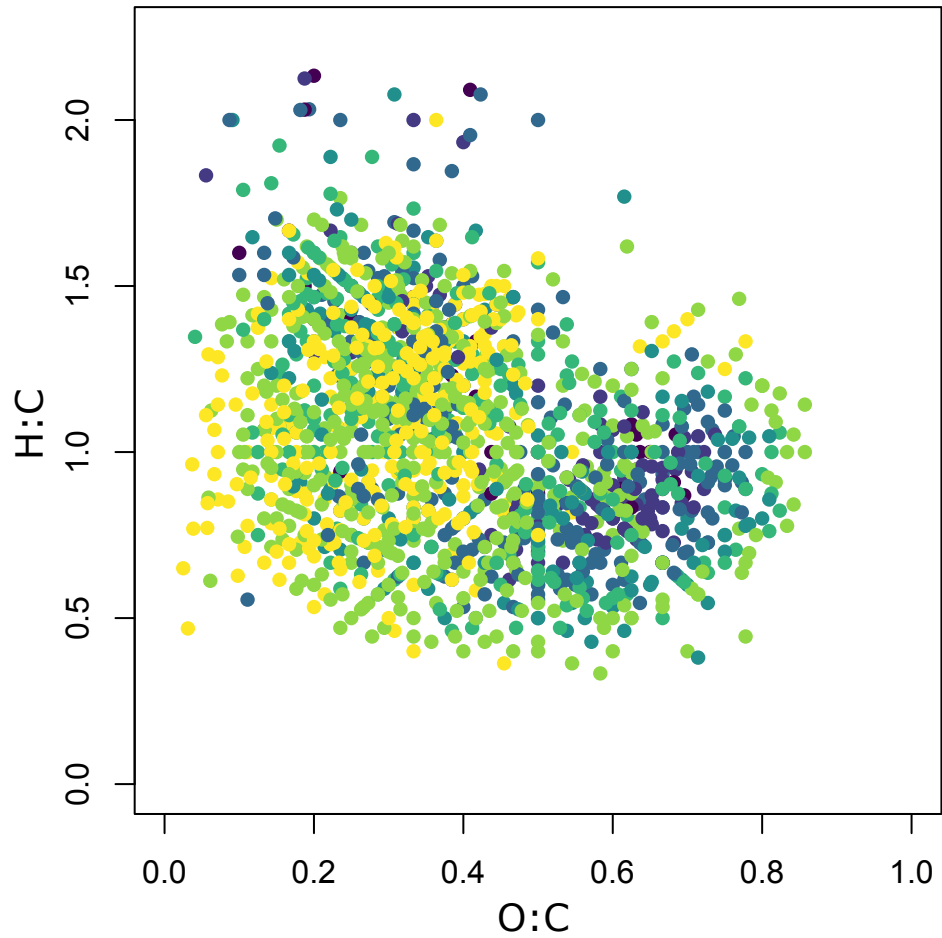


Figure 6.

